JOURNAL OF Materials CHEMISTRY

Electronic instabilities in compounds with hexagonal nets

Claudia Felser, Karena Thieme and Ram Seshadri

Institut für Anorganische Chemie und Analytische Chemie, Johannes Gutenberg-Universität, Mainz, Becher Weg 24, D-55099, Mainz, Germany

Received 12th October 1998, Accepted 20th November 1998

Ab initio band structure calculations on some compounds with either hexagonal or triangular nets in their crystal structures are presented. The view taken is that electronic instabilities as manifested in certain visualisations of the electronic structures can be indicative of the presence of interesting ground states including superconductivity. The Fermi surfaces of known hexagonal superconductors such as TaS_2, $Li_{0.5}NbO_2$ and the new superconductor, Li-doped β-ZrNCl have been examined for such patterns of instabilities. Similar patterns in the Fermi surfaces of other compounds with related structural motifs but of different compositions and/or electron counts have then been sought. Amongst the compounds so analysed are the metallic delafossite $PdCoO_2$, and SrPdP with the ZrBeSi structure.

Perhaps more than in any other branch of chemistry, the preparation of extended inorganic solids is often driven by the search for a specific property. Nonetheless, in most instances, the guidelines that one has for doing so are meagre. The problem is itself simply stated: using nothing but the Periodic Table of the elements, can a solid with a specific property be designed. The solid could perhaps belong to a new structure type, but more usually would be isostructural with known solids. The reason for the absence or paucity of suitable guidelines stems less from lack of effort and more from the sheer complexity of the problem. Indeed, even to predict the structure of the extended inorganic solid or solids that would be formed through the mixing of a few elements in some simple proportion has proved to be an open challenge.[1]

Rather than address the entire problem, one is then obliged to chose small subsets that might be more tractable. An example is the rule of thumb that materials show up interesting electronic properties in the vicinity of metal–insulator (M–I) transitions. A candidate system for an M–I transition is therefore selected and through suitable control of the composition or other physical parameter, the vicinity of the transition is explored for the specific property. This general idea has often proved successful in finding new superconductors. In the case of the recent findings of giant negative magnetoresistance (GMR) in certain perovskite manganites, the property associated with the M–I transition is itself rather novel.

There has been much interest in electronic instabilities associated with the square-net topology of atoms found in the cuprate high-T_C superconductors.[2,3] Through accurate band structure calculations backed up usually by high resolution angle-resolved photoemission experiments, it is now established that certain nesting motifs occurring simultaneously with highly disperse regions in the fermi surfaces (FS) of these compounds are good indicators of the superconducting properties. These ideas have in fact existed for many years in connection with the A15 superconductors.[4] Approaching this from another direction, the occurrence of similar nesting motifs in other compounds could be used as a guideline for finding new superconductors.

Comparing the electronic structures of some layered manganites and cuprates, we have recently suggested that the nesting motifs in the FS (a van Hove singularity) might point to properties other than superconductivity.[5] In the particular case of the layered manganite, despite its *spin-polarised* electronic structure (including the occurrence of van Hove singularities) being similar to the electronic structure of the isostructural superconducting cuprate, the different electron count results in the compound being magnetic rather than superconducting. Similarly, we have suggested that this van Hove singularity scenario might be applicable to valence instabilities in some Eu compounds.[6] In the system Ln_3S_4 (Ln = rare-earth) where such patterns of instabilities have been identified, replacing the rare-earth from La though Gd to Eu takes the system from being a superconductor, through a compound associated with an M–I transition and GMR, on to a valence unstable compound.

Our interest in this general problem has led us to ask the question whether these special patterns of electronic instabilities are exclusive to compounds with square nets or whether they can be found in compounds with hexagonal nets as well, and if so, whether they point to the possible existence of interesting ground states. Using the insights obtained from the electronic structures of 2*H*-$NbSe_2$, 2*H*-TaS_2, $LiNbO_2$,[7] and β-ZrNCl,[8] we propose the search for superconductivity in 3*R*-$PdCoO_2$ and SrPdP. Our strategy is to study some parent compound which might be insulating (ZrNCl for example) or metallic ($PdCoO_2$ for example). The correct number of holes or electrons are then 'doped' within a rigid band framework by demanding that suitable and proximal saddle points (SP) in the energy band structure (occurring at an energy E_{SP}) are brought into coincidence with the Fermi energy. Fermi surfaces are thus displayed as isosurfaces of some constant energy E_{SP}. Through an integration of the densities of state (the DOS) one can find the number of holes or electrons that bring about the coincidence of E_{SP} with E_F. In general, the validity of such rigid band 'doping' arises from the recovery of the chemically optimal doping, particularly if only one band crosses the E_F.

1 Crystal structures

Table 1 lists the crystal structure of the six compounds with hexagonal sheet motifs which have been used in the calculations presented here. The six compounds can be broadly classified into two structure types. The first comprise the early transition metal dichalcogenides, $LiNbO_2$ and the delafossite $PdCoO_2$. These are characterised by the presence of close-packed or nearly-close packed sheets of metal atoms in the structure. The delafossite $PdCoO_2$[9] in fact has two different transition metal atoms separately forming nearly close-packed sheets. TaS_2 and $NbSe_2$ have metal–chalcogenide trigonal prisms arranged in an edge shared manner in layers. The edge-sharing results in short metal–metal contacts. $LiNbO_2$ is a stuffed variant of this structure with sheets of edge-shared NbO_6 trigonal prisms. The Li atoms stuff the octahedral holes

Table 1 Crystal structures

$2H$-TaS_2, SG: $P6_3/mmc$ (no. 194) $a=3.316$ Å, $c=12.07$ Å			
Atom	x	y	z
Ta	1/3	2/3	1/4
S	1/3	2/3	0.621

$2H$-$NbSe_2$, SG: $P6_3/mmc$ (no. 194) $a=3.440$ Å, $c=12.482$ Å			
Atom	x	y	z
Nb	1/3	2/3	1/4
Se	1/3	2/3	0.616

$2H$-$LiNbO_2$, SG: $P6_3/mmc$ (no. 194) $a=2.9063$ Å, $c=10.447$ Å			
Atom	x	y	z
Li	0	0	1/2
Nb	1/3	2/3	1/4
O	1/3	2/3	0.62

$3R$-$PdCoO_2$, SG: $R\bar{3}m$ (no. 166) $a=2.83$ Å, $c=17.743$ Å			
Atom	x	y	z
Pd	0	0	0
Co	0	0	0.5
O	0	0	0.1112

$1T$-β-ZrNCl, SG: $P\bar{3}m1$ (no. 164) $a=3.605$ Å, $c=9.221$ Å			
Atom	x	y	z
Zr	−1/3	1/3	0.3586
N	1/3	−1/3	0.4150
Cl	0	0	0.1916

SrPdP, SG: $P6_3/mmc$ (no. 194) $a=4.118$ Å, $c=8.858$ Å			
Atom	x	y	z
Sr	0	0	0
Pd	1/3	−1/3	1/4
P	−1/3	1/3	1/4

between the sheets. The delafossite $PdCoO_2$ has slabs of edge-shared CoO_6 octahedra with Pd atoms occupying two-coordinate sites between these slabs. The panels of Fig. 1 display the structures of $2H$-$LiNbO_2$ and $3R$-$PdCoO_2$.

The other compounds discussed in this contribution, namely ZrNCl and SrPdP[10] are different. Rather than forming nearly close-packed sheets of metal atoms, SrPdP forms flat, graphitic sheets of Pd and P (alternating). The Sr atoms are between the sheets so formed. In ZrNCl, the sheets are formed from metal and N, and are buckled. Because of the buckling, they resemble the carbon atoms in the six-membered rings of the diamond (rather than the graphite) structure. The Cl atoms are between these buckled sheets resulting in a distorted trigonal antiprismatic environment of three N and three Cl around Zr. These trigonal antiprisms are further capped across one face by N. Because of the buckling in the sheets, the metal atoms are allowed to approach one another and the description of nearly close-packed sheets of metal atoms becomes once again applicable to this structure type. The structures of $3R$-ZrNCl and SrPdP are displayed in the panels of Fig. 2. We intend to discuss the electronic structures of ZrNCl in greater detail elsewhere, including problems associated with the structure.[11] Briefly, we have based our structure on a recent determination by Schleid and coworkers[12] of the structure of the isoelectronic compound $3R$-$NaZr_2N_2ClS$. This structure

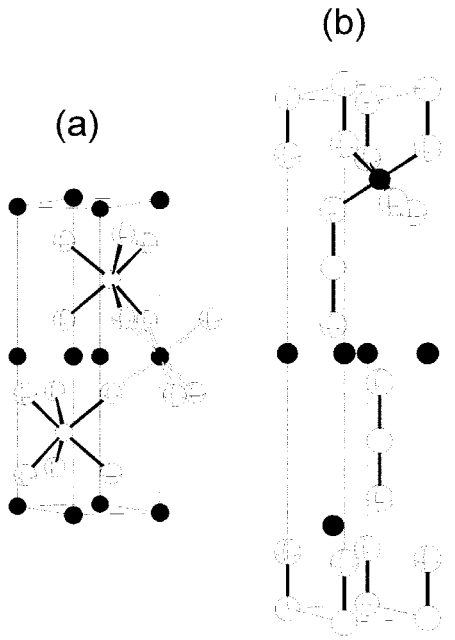

Fig. 1 Structures of (a) $LiNbO_2$ and (b) $3R$-$PdCoO_2$. The filled spheres represent Li or Co and the open spheres Nb or Pd. Oxygen atoms are represented as crossed spheres. The oxygen coordination around the metal atoms is indicated. The views are along nearly [110].

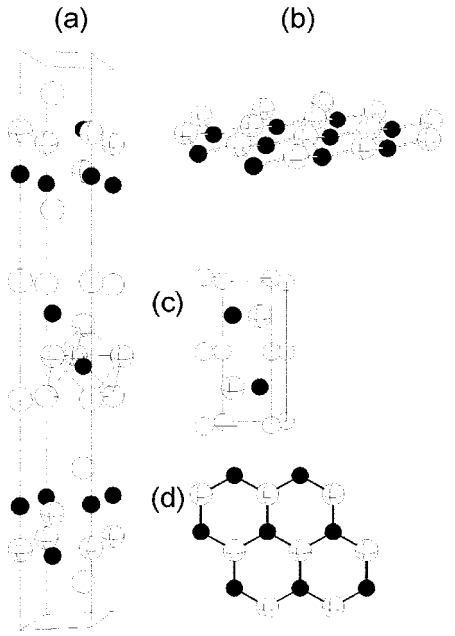

Fig. 2 (a) Structure of rhombohedral $3R$-β-ZrNCl following Schleid[12] projected along nearly [010]. The 3+3+1 coordination of Cl and N around Zr is indicated. Zr are black, Cl are large and open, and N are large and crossed. (b) View of a portion of the Zr–N slab in ZrNCl showing the buckled graphite (or diamondoid) net. (c) Structure of SrPdP. Pd is black, P is crossed and large and Sr is open. (d) The graphitic sheet of Pd and P in SrPdP seen down [001].

does not suffer the problem of the earlier one given by Juza and Friedrichsen[13] which had a very short Zr–Zr contact along the c-axis. These compounds have been recently been examined at the extended Hückel level by Woodward and Vogt.[14]

2 Calculation details

The central Brillouin zones for the different space groups that the compounds crystallise in are described in ref. 15. All the compounds except $3R$-$PdCoO_2$ crystallise in a primitive hexag-

onal space group (we have chosen to work with the primitive hexagonal polymorph instead of rhombohedral 3*R* ZrNCl). For this space group, the central Brillouin zone (BZ) is a wedge. Usually we consider only one circuit in the BZ described by the points Γ, K and M. The other circuit, A, H and L gives rise to nearly identical dispersions in *quasi*-2D compounds. The energy isosurfaces are presented for the complete wedge. For the rhombohedral compound, 3*R*-$PdCoO_2$, the BZ still resembles a wedge but two of the points in the hexagonal BZ, namely K and H are no longer special points in the BZ.

The self-consistent calculations reported here were performed using version 47 of the Stuttgart TB-LMTO-ASA program.[16] Detailed descriptions of the local density approximation, the local spin density approximation (LDA/LSDA) and the procedure by which reciprocal space integrations are performed and self-consistency is achieved can be found elsewhere.[17] The atomic sphere approximation (ASA) relies on the partitioning of space into atom-centred spheres as well as empty spheres, the latter being important for structures that are not close-packed. The blowing up of the volumes of the atomic spheres and the selection of the radii and positions of the empty spheres are handled automatically in the LMTO suite of programs with the caveat that atom-centred spheres do not have a volume overlap of more than 16%.[18] The number of irreducible *k* points used exceeded 400 in all the calculations.

We have used the so-called 'fat-band' representation,[19] to obtain the orbital character of some of the bands. In this representation, each band is decorated with a width that is proportional to the sum of the weights of the corresponding orthonormal orbitals. In all the band structures shown, 'pure' orbital character corresponding to 100% character of a certain type of orbital is represented by decorating bands with a thickness of 2.5% of the total energy scale.

3 Results

3.1 General discussion of bonding in compounds with hexagonal nets

In discussing the electronic structures of superconducting compounds, comparisons with the high-T_C cuprates are inevitable. The principal structural feature in the cuprates is the presence of square nets of atoms arranged as in a chess-board where black squares could correspond to squares of O atoms with a Cu atom at the centre and white squares could correspond to Cu-free squares of O atoms. When the Cu atoms are decorated with $d_{x^2-y^2}$ orbitals and the O atoms with p_x and p_y orbitals, one observes qualitatively that the bonding and antibonding states arising from the σ interaction can propagate freely through the planes. This is what gives rise to the remarkable dispersion of the bands derived from the Cu $d_{x^2-y^2}$ orbital in the high-T_C cuprates.[20] This disperse band in combination with certain patterns of instabilities is perhaps implicated in the unusually high T_C values in the cuprates. One would therefore seek disperse bands in the vicinity of the Fermi surfaces in other candidate superconducting compounds, in addition to the instabilities.

A close-packed plane of metal atoms with each atom surrounded by six others does indeed give rise to highly disperse bands arising from the metal–metal bonding. In compounds such as the layered dichalcogenides however, the bands due to metal d_{z^2} are in fact not very disperse. The reason can be found in the scheme presented by Hughbanks and coworkers[21] for the 3-center–2-electron (3c–2e) bonding in compounds such as MoS_2. The three-center bonding arises due to the metal atoms in the sheet having ligands over and under every second triangle. The result of such bonding is actually the localisation of electron density between every alternate triangle of metal atoms. The orbitals so formed have each two lobes with the same sign as depicted in Fig. 3(a). Suitable linear combination of the three orbitals lead to bonding, nonbonding and antibonding interactions. The effect of this type of localisation will manifest in some of the band structures discussed here.

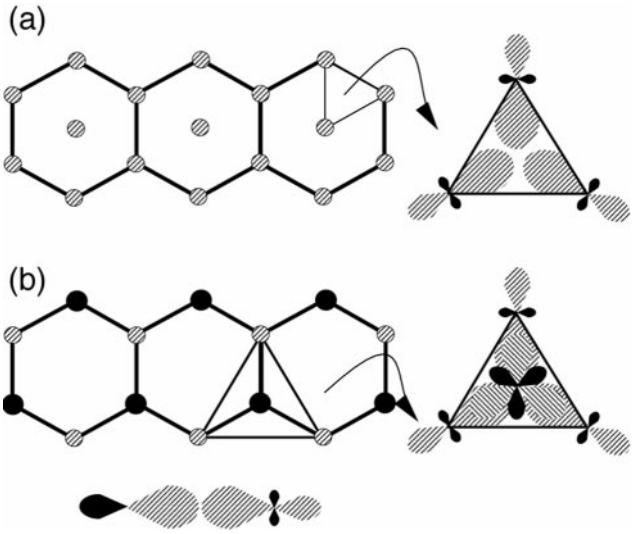

Fig. 3 (a) Transition metal atoms in a compound with close packed sheets of metal atoms ($LiNbO_2$ for example). Depending on the presence of a ligand, localised 3c–2e bonding within every alternate triangle is possible as displayed in the scheme with three sd^2 or d^3 orbitals. (b) Atoms in a compound with sheets of anions and cations (SrPdP for example). Where the bonding is localised in panel (a), one can stuff an anion to obtain the 2c–2e bonding scheme in panel (b) involving sp^2 anion orbitals and d^3 cation orbitals.

In our present study, we also consider some systems which could be regarded as 'stuffed' hexagonal nets. Such stuffing then yields the sheet structure observed in SrPdP where a planar net is formed from Pd and P atoms with each Pd being coordinated to three P and each P coordinated to three Pd. The result of this is a distinct, highly covalent, bonding pattern in the metal atom plane. The orbital scheme for such a plane is depicted in Fig. 3(b).

ZrNCl is somewhere in between. Firstly, it comprises *double* sheets of metal atoms and metal–metal interactions perpendicular to the sheet direction could be important. Secondly, because the sheets (of Zr–N) are like in SrPdP but buckled, both metal–metal interactions as well as metal–N interactions are likely to be important as far as the electronic structure of the sheet is concerned.

Following Savin *et al.*[22] we visualize the localisation by using the electron localisation function (ELF)[23] to decorate the charge density in the plane. This function represents the (suitably scaled) complement of the probability of finding in a certain region of the real space, two electrons of like spin. High localisation in conjunction with high valence charge density therefore represents a chemical bond. We consider different representations of the ELF of $LiNbO_2$ presented in Fig. 4. Panel (a) of this figure depicts the total electron localisation in the Nb plane, including core and valence electrons. The colouring of the extent of localisation is indicated in the figure. Looking at the oxygen plane in panel (b) of this figure, we observe that the localisation in the Nb triangles takes place in those triangles that *do not* have oxygen above and below them. Panel (c) of this figure depicts an isosurface of constant electron density around the Nb plane, for a density value of 0.025 e $Å^{-3}$. This isosurface has then been decorated by the valence electron localisation. Again, it is seen that Nb_3 triangles that do not have O above and below them are possessed not only of regions of high localisation but also of electron density. What is interesting is that we now

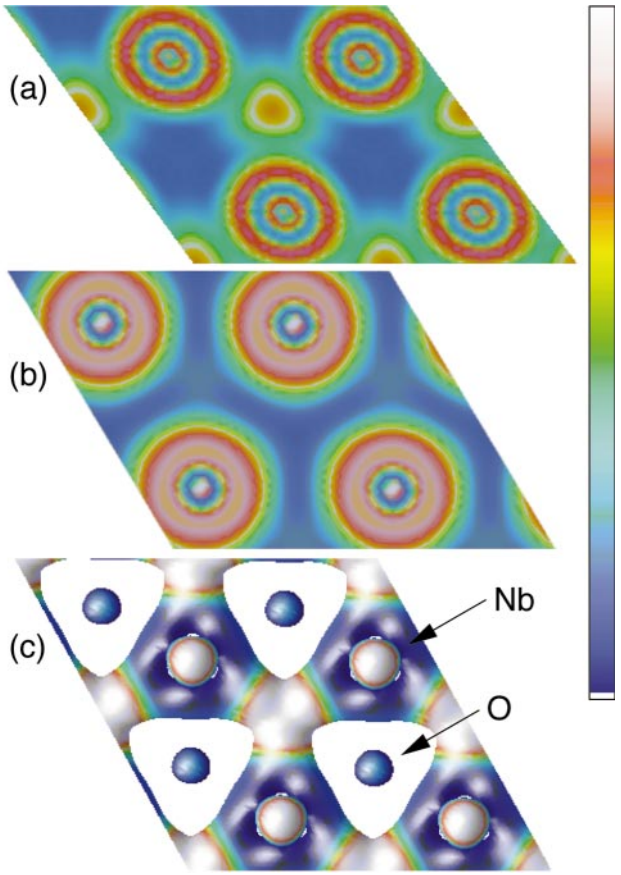

Fig. 4 (a) Total electron localisation displayed in the Nb plane of $LiNbO_2$. The colour coding runs from deep blue (delocalised) through red and yellow to white (maximum localisation) as indicated in the bar on the right. Every alternate triangle formed by the Nb is seen to possess high localisation. (b) Total electron localisation in the O plane of $LiNbO_2$. From this figure, it is seen that the only the Nb triangles that do not have O above and below are possessed of high localisation. (c) Electron density isosurface (0.025 e $Å^{-3}$) in the Nb layer decorated by the valence ELF.

also see some valence electron localisation above and below the Nb atoms. This arises from the occupied d_{z^2} orbital on Nb. Where there is high electron density associated with high localisation between the metal atoms one could stuff in a ligand. In fact, in certain layered compounds such as GdI_2, anion insertion (in this case hydrogen) actually follows this topochemical nature.[24]

Such anion stuffing also leads to the structure of the metal–anion sheets in compounds such as SrPdP. The ELFs are shown in Fig. 5, with panel (a) depicting the total ELF in the Pd–P sheet and panel (b), the electron density isosurface (for an isosurface value of 0.025 e $Å^{-3}$) decorated by the valence electron ELF. The ELF of the 3c–2e bonding now has a core because it is a real atom. The significant difference is that the electrons on Pd for this isosurface value are not localised. Neither is the ELF near the P atom as localised as the ELF within the metal triangles in the previous case. This is in agreement with the nature of the highly disperse conduction bands of SrPdP that we shall examine presently.

3.2 The layered dichalcogenides TaS_2 and $NbSe_2$ and $LiNbO_2$

2*H*-TaS_2 and 2*H*-$NbSe_2$ are superconductors[25] with T_C values of 0.8 and 7.3 K, respectively. $LiNbO_2$ is isoelectronic with MoS_2 and is a band insulator for the same reason that MoS_2 is a band insulator—that the valence band is constructed from d_{z^2} orbitals, this is filled with two electrons and well separated from other d-orbital derived bands because of the trigonal prismatic environment of Nb. Deintercalation of some

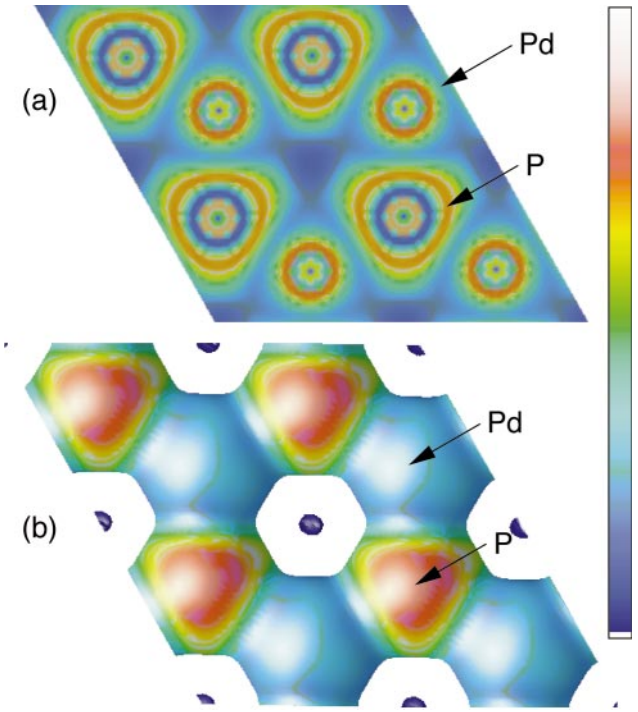

Fig. 5 (a) Total electron localisation displayed in the Pd–P plane of SrPdP. (b) Electron density isosurface (0.025 e $Å^{-3}$) in the Pd–P sheet decorated by the valence ELF. The colour bar is indicative of the degree of localisation as in the previous figure.

of the Li to reach compositions close to $Li_{0.5}NbO_2$ results in a half-filled d_{z^2}, conductivity and a transition to a superconducting state below 5 K. Hole doped $LiNbO_2$ in fact displays a band structure rather similar to the band structures of TaS_2 and $NbSe_2$. The band structures of TaS_2, $NbSe_2$[26] and $LiNbO_2$[27] are known, so we discuss the band structure only from the viewpoint of the instabilities therein.

Fig. 6 compares the band structure of these three compounds in a window around the Fermi energy. The d_{z^2} derived bands have been decorated with a width, whereby 100% d_{z^2} character corresponds to a width that is 2.5% of the displayed energy scale. TaS_2 and the isostructural compounds are layered. The low dimensionality is seen in the band structures as a smaller dispersion of all bands in the direction perpendicular to the slabs. Despite the anisotropic transport properties, the chalcogenide band has a significant three dimensional part. Especially

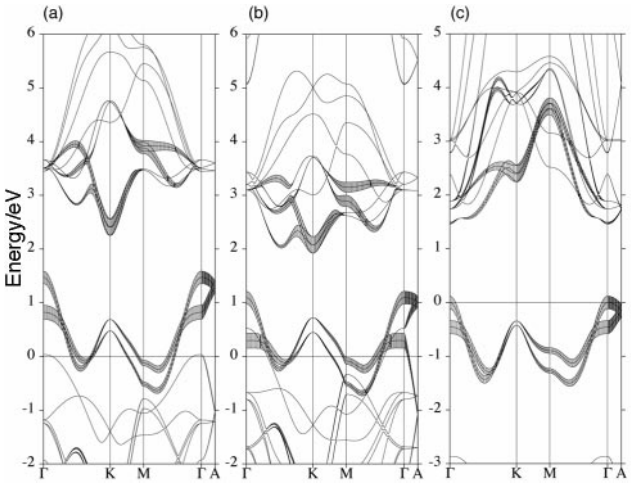

Fig. 6 (a) Band structure of 2*H*-TaS_2 showing the 1/2-filled Ta d_{z^2} orbital-derived fatband. (b) The 1/2-filled Nb d_{z^2} orbital-derived fatband of 2*H*-$NbSe_2$. (c) The filled Nb d_{z^2} orbital-derived fatband of $LiNbO_2$.

the chalcogenide band which crosses E_F has high dispersion along the direction perpendicular to the layers namely along Γ to A. The dispersion of the metal bands around and above E_F is small perpendicular to the slabs. The overlap of the metal and the chalcogenide states in the chalcogenides is significant while in $LiNbO_2$ there is a gap between O and Nb states.

In layered compounds the so called van Hove singularities (vHS) are common,[3] so we expect to see them in the band structure of these compounds. In TaS_2 and $NbSe_2$, we observe pairs of saddle points for the d_{z^2} bands. One pair of saddle points in TaS_2 is in the vicinity of the Fermi energy at a low symmetry point along the line between Γ and K, 0.082 and 0.23 eV below E_F. A second saddle point pair is situated 0.13 and 0.52 eV below E_F just at the M point in the case of TaS_2. In $NbSe_2$ the saddle points between Γ and K are situated 0.08 and 0.22 eV below E_F and the saddle points at M are situated 0.08 and 0.5 eV below E_F.

In $LiNbO_2$ only one pair of saddle points is found. Because of the band behaviour, the minima between Γ and K are now true minima. The first saddle point is situated just at E_F for a composition $Li_{0.4}NbO_2$ nearly 1 eV below E_F for $LiNbO_2$ at the M point.

3.3 The delafossite $PdCoO_2$

The band structure of $PdCoO_2$ and the bonding interactions have been described by us in detail elsewhere.[28] In Fig. 7(a), we show the band structure of this compound with the Pd d_{z^2} band decorated in a small energy window around the E_F. The band structure of this compound looks rather different from the one previously discussed. The interesting bands are derived from Pd. From the composition, we expect Pd to be monovalent and Co to be trivalent. $PdCoO_2$ is a metal because the Pd d_{z^2} is only half occupied and crosses E_F. The trivalent Co is low spin and non-magnetic with occupied Co t_{2g} separated from empty Co e_g that are above E_F. Instead of d^1, we have here a d^9 system. Whereas in TaS_2 the bonding metal–metal band of the d^3 orbitals crosses E_F (with the main contribution from d_{z^2}), here it is the corresponding metal–metal antibonding band that crosses E_F. Again the main contribution is from Pd d_{z^2}, but with small contributions also from $d_{x^2-y^2}$ and d_{xy}.

The most significant difference of this compound compared with the chalcogenides and $LiNbO_2$ discussed previously is that the metal–metal interaction within the planes is not localised. This perhaps arises because of the arrangement of the ligands. The chalcogenides are above and under every second triangle of the metal atoms in the dichalcogenides. The same arrangement of O holds in $LiNbO_2$. In $PdCoO_2$, however, the O ligands from the cobalt–oxygen octahedra are directly above and below the two-coordinate Pd. Therefore localisation associated with half occupied 3c–2e bonding orbitals is not found and the metal–metal interaction is delocalised all over the plane. As a result, the overall dispersion of the d_{z^2} or one of the d^3 bands is significantly higher in this compound.

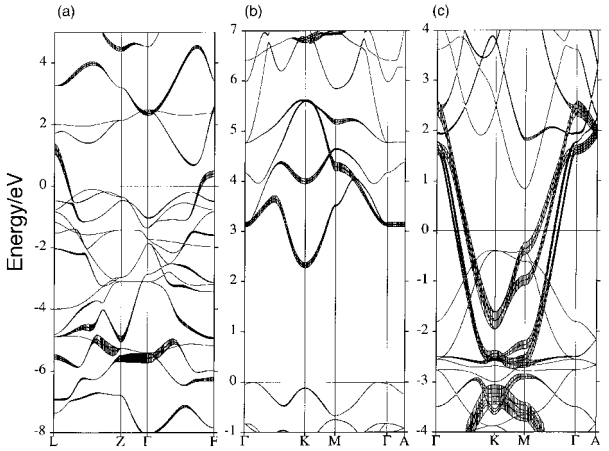

Fig. 7 (a) Band structure of 3*R*-$PdCoO_2$ showing the Pd d_{z^2} fatband. (b) The empty $d_{x^2-y^2}$ conduction fatband of hexagonal *β*-ZrNCl. (c) The Pd–P σ and σ* fatbands of SrPdP.

In general this compound is a candidate for interesting electronic properties, combining an anisotropic electronic structure and d^9 palladium. We have therefore investigated very carefully the electronic structure around E_F. In this compound, a saddle point at the F point in the vicinity of the Fermi energy is found. An electron doping of 0.3 e per formula unit would bring about the coincidence of the Fermi energy with the saddle point and perhaps result in superconductivity.

3.4 The 'stuffed' hexagonal nets of ZrNCl and SrPdP

The layered compound *β*-ZrNCl can be Li-intercalated between the double sheets to yield superconducting compounds with T_C values in the range 15 K.[8] In the isostructural Hf compounds, the T_C is as high as 25 K.[29] In Fig. 7(b) the $d_{x^2-y^2}$ conduction fatband of hexagonal *β*-ZrNCl is displayed. We can once again find three d^3 bands in this compound corresponding to the metal plane. The strength of the bonding and the eigenvector contributions to the band are considerably affected by the bonding of Zr and N. The band nearest to E_F is mainly derived from $d_{x^2-y^2}$ and d_{xy} (not shown) with the contribution from d_{z^2} being pushed up because of the capping N atom in the coordination polyhedron around Zr. The saddle point as in the other compounds is again found at the M point.

In SrPdP where Pd and P are really in one plane, the metal–metal interaction is replaced by a metal-nonmetal interaction mediated by the d^3 orbital on Pd and the sp^2 orbitals on P. The introduction of the non-metal leads to two 2c–2e bonding interactions with corresponding σ and π type bands. In Fig. 7(c), we display the σ and σ* fatband of SrPdP. SrPdP is a metal with σ* derived bands crossing E_F. Again the bands are nearly doubly degenerate, because there are two formula units per primitive unit cell. The remarkable dispersion of the conduction band arises from the special nature of the bonding as seen in considering the ELFs. The σ* bands lead again to a pair of saddle points at the M point in the BZ. It is the same saddle point that in fact has been implicated in the inhomogeneous mixed-valence behaviour of EuPdP.[6]

3.5 The energy isosurfaces

The energy isosurfaces of the six compounds discussed here (corresponding to the Fermi surfaces of the 'doped' compounds) are displayed in the panels of Fig. 8. The level of 'doping' and the energies of the corresponding saddle points are presented in Table 2. The isosurfaces have been decorated with the Fermi velocities with hotter colours (red, orange, yellow) corresponding to regions of high Fermi velocities, and colder colours (green, blue) corresponding to regions of low Fermi velocity.

For TaS_2 and $NbSe_2$, Fermi surfaces of the hole doped compounds at the first saddle point are displayed. These compounds have typical two dimensional Fermi surfaces with two envelopes corresponding to the nearly double degenerated band. In the figure, it actually looks like a single envelope because the bands are truly degenerate at the edges of the BZ. A third band which crosses E_F in TaS_2 and $NbSe_2$, which is a chalcogenide p band leads to the three dimensional envelope around Γ, giving the compound some three dimensional character despite its anisotropic transport properties.

Because of the two pairs of saddle points in the band structure we find also two different instabilities in the isosurfaces of TaS_2 and $NbSe_2$. The first is an X-shaped nesting

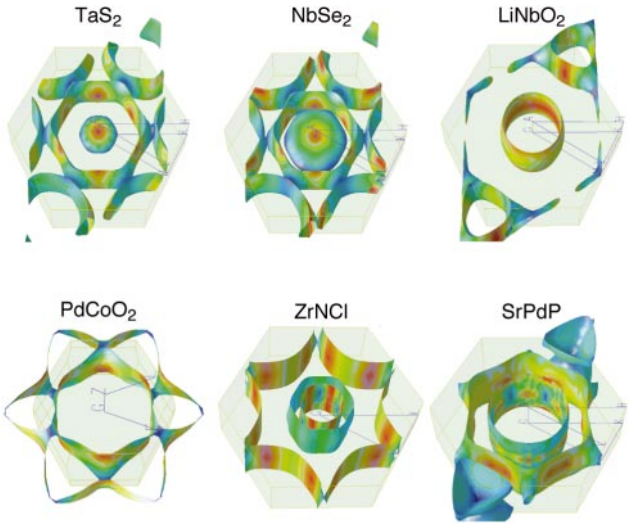

Fig. 8 Energy isosurfaces (Fermi surfaces of the 'doped' compounds) of the six compounds discussed in the text displayed at energies that bring nearby saddle points into coincidence with the Fermi energy. The surfaces have been coloured with the Fermi velocities, with the hot colours (red, orange, yellow) representing high Fermi velocities and the colder colours (blue, green) representing low Fermi velocities.

Table 2 Energies of the nearby saddle points and doping level

Compound	E (first SP)/eV	e-doping
2*H*-TaS_2	−0.08	−0.26
2*H*-$NbSe_2$	−0.08	−0.25
$LiNbO_2$	−0.91	−0.60
$PdCoO_2$	+0.40	+0.28
ZrNCl	+3.50	+0.55
SrPdP	−0.35	−0.41

(blue regions) that is nearly doubly degenerate, and is found along the Γ to K or A to H directions. The latter is not shown in the band structure. The second is not so easy to recognise, because it is situated at the edge of the BZ at the M point. We therefore see only half of the X of the X-shaped nesting. A saddle point is a flat region in the band structure and therefore the Fermi velocity is low, and the colour of the Fermi surface is blue at these points. Regions of high dispersions corresponding to higher Fermi velocity are also seen in our visualisation. Nevertheless, if we compare the overall dispersion of the bands which cross E_F with the overall dispersion of the corresponding Cu–O band in the cuprate superconductors, we can clearly seen that there are major differences. Within our general scheme, this would provide qualitative reasons for the lower T_C values in these compounds.

In $LiNbO_2$ the overall Fermi surface is more two dimensional than the chalcogenides. The O states are well separated in energy from the metal states resulting in a gap between the corresponding states. We find only the nesting at the M point, as expected from the band structure. In the corresponding energy isosurface, we can clearly seen again the X-shaped nesting at the M point.

For $PdCoO_2$, in agreement with the band structure, the isosurface is slightly more three dimensional than the isosurface of $LiNbO_2$. This is seen for example in the dispersion along the Γ–Z direction. Despite the different BZ, the nesting patterns are similar with blue regions being found at one edge of the BZ. Apart from the blue regions, in this compound also, we find regions of high dispersions which are coloured in the hotter colours.

ZrNCl seems to have the largest anisotropy as seen in the isosurface. This is despite the metal–metal interaction between the slabs in the double Zr–N layer. However, this metal–metal interaction is restricted in extent so it cannot form disperse bands. From our knowledge of the band structure, three bands cross the energy corresponding to the saddle point so the isosurface shows three envelopes. There is again nesting at the M point but the same band that gives rise to the nesting also shows regions of relatively high dispersion which are seen as reddish-orange regions.

In SrPdP, two nearly degenerate pairs of σ* cross the isosurface. The first degenerate σ* band forms a cylinder around Γ. The second gives rise to a hexagon without dispersion in the Γ–A direction, building a saddle point at M. The nesting is again blue and X-shaped. This same band has highly disperse regions. The third pair of degenerate bands are π* and result in an envelope which looks rather different. Because this π* band has a minimum just at the K point, we observe the triangular objects with localised but three dimensional character. We note that these localised features are displayed only at two corners of the BZ and not at four others, where they are also found for symmetry reasons.

4 Discussion

Compounds with interesting electronic properties, particularly those displaying superconductivity, show up instabilities in suitable visualisations of the electronic structure. The patterns of instabilities in compounds with hexagonal nets of metal atoms are not unlike those found in compounds with square nets such as the high-T_C cuprates, the distinguishing feature being an X-shaped nesting in combination with highly disperse regions in the isosurfaces (of Fermi surfaces). Indeed, we find that from the viewpoint of the features that we believe to be important for superconductivity, the difference in the electronic structures of the compounds considered here and those of the cuprate high-T_C superconductors is largely one of degree. A significant difference in some compounds with hexagonal nets of metal atoms is the occurrence of 3c–2e bonding and the resulting narrowing of the conduction band. From the present work, we suggest that this could be avoided in two ways: the first is to ensure that the ligand coordinates to the metal atoms from a direction normal to the metal atom plane as in the delafossites. The second is to stuff the metal atom plane with anions giving rise to 2c–2e bonding rather than 3c–2e bonding. We suggest that the identification of the requisite patterns of instabilities can provide guidelines to the synthesis of new superconductors.

In the superconducting compositions examined here, in keeping with the van Hove scenario, the T_C seems to be related to the position of the SP with respect to the E_F. Simultaneously, a highly disperse conduction band seems to be necessary for high T_C. A third point is the dimensionality and ZrNCl is the compound amongst the ones discussed here that simultaneosly has the highest disperse bands, a suitable instability and the greatest 2D character. These could be the reasons why it also displays the highest T_C. While we find disperse and localised bands in all the band structures, the overall dispersions of the bands of the known superconductors dealt with here are lower than in the high-T_C cuprates. The localisation within the metal triangles influences the dispersion in all the compounds except the speculative systems SrPdP and $PdCoO_2$ where we believe superconductivity could be achieved through suitable doping.

An important aspect of this contribution is the analysis of the nature of bonding in systems with triangular or hexagonal nets of metal atoms in the structure and we can carry this analysis futher through examining the so called d^3 fatbands (comprising metal $d_{x^2-y^2}$, d_{xy} and d_{z^2}) across the series $LiNbO_2$, ZrNCl and SrPdP. These are shown in the panels of Fig. 9. We choose these compounds because they represent different

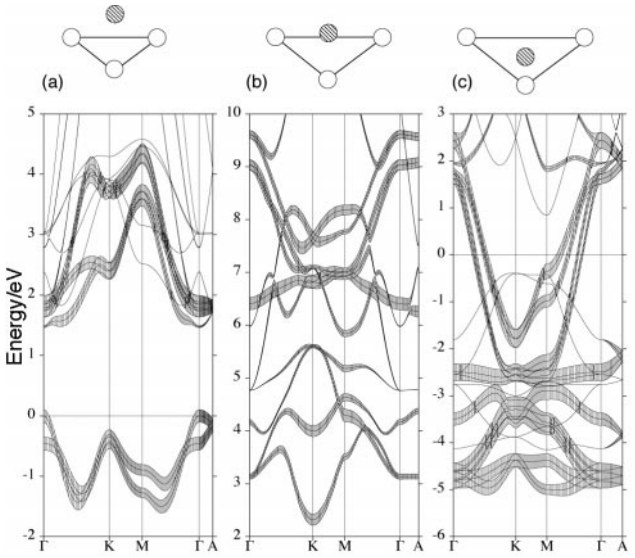

Fig. 9 d^3 fatbands (with orbital contributions from metal $d_{x^2-y^2}$, d_{xy} and d_{z^2}) of (a) $LiNbO_2$, (b) ZrNCl and (c) SrPdP. The schemes of the atoms above the band structures show the coordination change from a metal triangle capped by a ligand, through a squashed cap, to a triangle with the ligand at the centre.

degrees of capping of the metal triangles with the ligand as indicated in the schemes above each band structure. In $LiNbO_2$, the capping ligand is some distance from the metal triangle and the 3c–2e scheme of Hughbanks and coworkers[21] is fully applicable. The d^3 fatbands are clearly separated into a bonding part centered around -1 eV and an antibonding part centered around 3 eV (both energies with reference to the E_F). SrPdP [Fig. 9(c)] forms the end member of this series with the ligand in the plane of the metal triangle. It has σ bonding states between -5 and -3.5 eV, separated from σ* states between -2 and 2 eV. In between, centered around -3 eV are non-bonding states. In the intermediate capping case of ZrNCl [Fig. 9(b)], where the N atoms are only slightly above the metal triangle, σ and π bonding states are mixed so the separation between the different kinds of bonding is less clear. Nonetheless, there is a visible evolution in the nature of the d^3 bands as the nature of the ligand capping is changed, and this we believe would be important from the viewpoint of superconductivity.

5 Acknowledgements

Professor O. K. Andersen, Dr. O. Jepsen and Dr. A. Burkhardt are thanked for providing the LMTO codes and for their continued support. We are particularly grateful to Dr. Hj. Mattausch for pointing out the problem of the structure of β-ZrNCl. R. J. Cava and W. Tremel are thanked for discussions and encouragement. Financial support from the Fonds der chemischen Industrie and the Deutsche Forschungsgemeinschaft is acknowledged.

References

1 J. Maddox, *Nature*, 1988, **335**, 201; J. Pannetier, J. Bassas-Alsina, J. Rodriguez-Carvajal and V. Caignaert, *Nature*, 1990, **346**, 343.
2 J. Labbé and J. Bok, *Europhys. Lett.*, 1987, **3**, 1225.
3 D. M. Newns, H. R. Krishnamurthy, P. C. Pattnaik, C. C. Tsuei, C. C. Chi and C. L. Kane, *Physica B*, 1993, **186**, 801.
4 J. Labbé and J. Friedel, *J. Phys. (Paris)*, 1966, **27**, 153.
5 C. Felser, R. Seshadri, A. Leist and W. Tremel, *J. Mater. Chem.*, 1998, **8**, 787.
6 C. Felser, S. Cramm, D. Johrendt, A. Mewis, O. Jepsen, G. Hohlneicher, W. Eberhardt and O. K. Andersen, *Europhys. Lett.*, 1997, **40**, 85.
7 M. J. Geselbracht, T. J. Richardson and A. M. Stacey, *Nature*, 1990, **345**, 324.
8 S. Yamanaka, H. Kawaji, K. Hotehama and M. Ohashi, *Adv. Mater.*, 1996, **9**, 771; H. Kawaji, K. Hotehama and S. Yamanaka, *Chem. Mater.*, 1997, **9**, 2127.
9 R. D. Shannon, D. B. Rogers and C. T. Prewitt, *Inorg. Chem.*, 1971, **10**, 713; C. T. Prewitt, R. D. Shannon and D. B. Rogers, *Inorg. Chem.*, 1971, **10**, 719; D. B. Rogers, R. D. Shannon, C. T. Prewitt and J. L. Gillson, *Inorg. Chem.*, 1971, **10**, 723.
10 D. Johrendt and A. Mewis, *Z. Naturforsch.*, *Teil B*, 1990, **45**, 1262.
11 C. Felser and R. Seshadri, *J. Mater. Chem.*, in press.
12 F. Lissner and T. Schleid, Poster presented at the DFG Solid State Chemistry Symposium, Saarbrücken, Germany, 1998.
13 R. Juza and H. Friedrichsen, *Z. Anorg. Allg. Chem.*, 1966, **622**, 123.
14 P. M. Woodward and T. Vogt, *J. Solid State Chem.*, 1998, **138**, 207.
15 C. J. Bradley and A. P. Cracknell, *The mathematical theory of symmetry in solids*, Clarendon Press, Oxford, 1972.
16 O. K. Andersen and O. Jepsen, *Phys. Rev. Lett.*, 1984, **53**, 2571; O. K. Andersen, Z. Pawlowska and O. Jepsen, *Phys. Rev. B*, 1986, **34**, 5253; O. K. Andersen, O. Jepsen and D. Glötzel, in *Highlights in Condensed-Matter Theory*, ed. F. Bassani, F. Fumi and M. P. Tosi, North-Holland, New York, 1985.
17 H. L. Skriver, *The LMTO method*, Springer, Berlin, 1984.
18 G. Krier, O. Jepsen and O. K. Andersen, unpublished results.
19 O. Jepsen and O. K. Andersen, *Z. Phys. B*, 1995, **97**, 35.
20 W. E. Pickett, *Rev. Mod. Phys.*, 1989, **61**, 433.
21 Y. Tian and T. Hughbanks, *Inorg. Chem.*, 1993, **32**, 400; K. A. Yee and T. Hughbanks, *Inorg. Chem.*, 1991, **30**, 2321.
22 A. Savin, R. Nesper, S. Wengert and T. F. Fässler, *Angew. Chem.*, 1997, **109**, 1893; *Angew. Chem.*, *Int. Ed. Engl.*, 1997, **36**, 1809.
23 A. D. Becke and N. E. Edgecombe, *J. Chem. Phys.*, 1990, **92**, 5397.
24 C. Michaelis, W. Bauhofer, H. Buchkremer-Hermanns, R. K. Kremer, A. Simon and G. J. Miller, *Z. Anorg. Allg. Chem.*, 1992, **618**, 98.
25 L. Bulaevski, *Sov. Phys. Usp.*, 1976, **18**, 514.
26 L. F. Mattheiss, *Phys. Rev. B*, 1973, **8**, 3719; G. Y. Guo and W. Y. Liang, *J. Phys. C. Solid State Phys.*, 1987, **20**, 4315.
27 D. L. Novikov, V. A. Gubanov and V. G. Zubkov, *Phys. Rev. B*, 1994, **49**, 15830.
28 R. Seshadri, C. Felser, K. Thieme and W. Tremel, *Chem. Mater.*, 1998, **10**, 2189.
29 S. Yamanaka, K. Hotehama and H. Kawaji, *Nature*, 1998, **392**, 580.

Paper 8/07896C